Applied Catalysis B: Environmental 91 (2009) 135–143

Contents lists available at ScienceDirect

Applied Catalysis B: Environmental

journal homepage: www.elsevier.com/locate/apcatb

Solvothermal preparation, electronic structure and photocatalytic properties of $PbMoO_4$ and $SrMoO_4$

Jinhong Bi, Ling Wu *, Yongfan Zhang, Zhaohui Li, Junqian Li, Xianzhi Fu *

State Key Laboratory Breeding Base of Photocatalysis, Research Institute of Photocatalysis, Fuzhou University, Fuzhou 350002, PR China

ARTICLE INFO

Article history:
Received 15 January 2009
Received in revised form 7 May 2009
Accepted 13 May 2009
Available online 20 May 2009

Keywords:
Solvothermal process
Photocatalytic activity
Salicylic acid
$PbMoO_4$
$SrMoO_4$
Electronic structure

ABSTRACT

$PbMoO_4$ and $SrMoO_4$ particles were successfully prepared via a simple solvothermal process. The obtained samples were characterized by X-ray diffraction, Brunauer–Emmett–Teller (BET) surface area analysis, UV–vis diffuse reflectance spectroscopy, scanning electron microscopy and a photoluminescence technique with terephthalic acid. The as-prepared $PbMoO_4$ samples show different photocatalytic activities for salicylic acid under UV light irradiation. $PbMoO_4$ exhibits relatively high photocatalytic activity for salicylic acid, Rhodamine B and benzene. While, $SrMoO_4$ possessing a similar structure to $PbMoO_4$ shows negligible photocatalytic activity though they exhibit similar BET surface areas and morphologies. Theoretical calculations reveal that $PbMoO_4$ contains higher dispersive valence and conduction bands than $SrMoO_4$. The highly dispersive valence and conduction bands can lead to higher mobility of the photo-generated carries and therefore a better photocatalytic activity.

1. Introduction

Semiconductor metal oxide photocatalysts have been widely employed in the treatment of all kinds of organic contaminants. Photocatalysis has many advantages over other treatment methods. It is environmentally friendly, capable of performing at room temperature, and can treat organic pollutants at extremely low concentrations. Photocatalysis of metal oxides is controlled by three processes. The first is the formation of photoexcited charges under light illumination, the second is charge transfers to the surface without recombination, and the third is the transfer to the reactants adsorbed on the surface. It has been reported that the second is associated with the prevention of the recombination of the photoexcited charges, which related to electronic structure. Therefore, the effect of electronic structure on the photocatalytic activity has attracted many researchers' interest [1,2].

Scheelite-structured compounds belonging to the molybdate families possess attractive luminescence and interesting structural properties. Because of their physical and chemical properties they are used as several technological applications such as scintillators [3], laser-host materials [4], cryogenic detectors for dark matter [5], or heterogeneous catalysts [6]. $PbMoO_4$ and $SrMoO_4$ crystallize in this so-called scheelite structure [7], which belong to the tetragonal space group $I4_1/a$ as shown in Fig. 1. They have been reported due to the above mentioned applications. $PbMoO_4$ has also been reported as a photocatalyst for the splitting of water [8,9]. There are several processes for preparation of $PbMoO_4$ and $SrMoO_4$ such as solid-state sintering [10], Czochralski method [11,12], hydrothermal method [13,14], etc. Our previous research showed that Bi_2MoO_6 prepared by a simple solvothermal process exhibited relatively high photocatalytic activities for the decomposition of the organic dyes [15]. Muktha et al. also reported that $BaBi_2Mo_4O_{16}$ could decompose organic pollutes [16]. Further researches for other molybdates to use as photocatalysts for the decomposition of the organic pollutes may proceed and the relationship between their structures (crystal structure and electronic structure) and photocatalytic activities should be demonstrated.

In the present study, $PbMoO_4$ and $SrMoO_4$ particles were prepared by a simple solvothermal process. The optimal experiment conditions for the preparation were investigated to get the high photocatalytic activity. In order to demonstrate the reason for the induced difference in photocatalytic activity between $PbMoO_4$ and $SrMoO_4$, the electronic structures of $PbMoO_4$ and $SrMoO_4$ were revealed by density functional theory calculations.

2. Experimental

2.1. Catalyst preparation

2.1.1. Synthesis of $PbMoO_4$ samples

$PbMoO_4$ was synthesized by a simple solvothermal process and a solid-state sintering. In the solvothermal process, $Pb(NO_3)_2$ and

* Corresponding authors. Tel.: +86 591 83738608; fax: +86 591 83738608.
E-mail addresses: wuling@fzu.edu.cn (L. Wu), xzfu@fzu.edu.cn (X. Fu).

0926-3373/$ – see front matter © 2009 Elsevier B.V. All rights reserved.
doi:10.1016/j.apcatb.2009.05.016

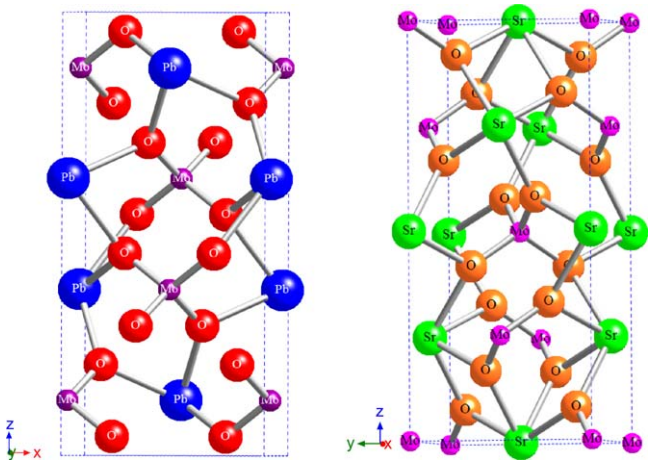

Fig. 1. Three-dimensional crystal structures of $PbMoO_4$ and $SrMoO_4$ with unit cells.

$(NH_4)_6Mo_7O_{24}{\cdot}4H_2O$ were used as the starting materials without further purification. The starting materials were added into a Teflon-lined steel autoclave of 100 mL. Then 20 mL of ethylene glycol was added. Under stirring, 4 mol/L of NaOH solution was used to adjust pH, and the autoclave was heated under autogenous pressure at 160 °C for 12 h at a series of different pH values (pH 5, 7, 9, 11). Afterward, the autoclave was cooled to room temperature gradually. The resulting solid powders were collected, and washed with deionized water and ethanol. Then they were dried at the room temperature. White powders were obtained except the sample prepared with pH 5. It exhibited a brown color. The samples prepared at different pH values of 5, 7, 9, 11 are denoted as $PbMoO_4$ (CS-5), $PbMoO_4$ (CS-7), $PbMoO_4$ (CS-9) and $PbMoO_4$ (CS-11), respectively. Another attempt to prepare $PbMoO_4$ was via solid-state sintering. Reagent grade oxides of PbO and MoO_3 were stoichiometrically mixed and ground carefully. The resulting powders were pressed into pellets and sintered at 200 °C for 1 h, 600 °C for 1 h and 1000 °C for 30 h. This sample is denoted as $PbMoO_4$ (SS).

2.1.2. Synthesis of $SrMoO_4$ sample

$SrMoO_4$ was also prepared via the solvothermal process with $Sr(NO_3)_2$ and $(NH_4)_6Mo_7O_{24}{\cdot}4H_2O$ as precursors under the condition of pH 9. The obtained sample is denoted as $SrMoO_4$ (CS-9).

2.2. Catalyst characterization

The as-prepared samples were characterized by powder X-ray diffraction (XRD) on a Bruker D8 Advance X-ray diffractometer at 40 kV and 40 mA with Ni filtered Cu Kα radiation. Data were recorded at a scan rate of 0.02° $2\theta\,s^{-1}$ in the 2θ range 17–60°. Brunauer–Emmett–Teller (BET) surface area was measured by using ASAP2020M from Micromeritics Instrument Corporation. UV–vis diffuse reflectance spectra (UV–vis DRS) of the samples were obtained for the dry-pressed disk sample using a UV–vis spectrophotometer (Cary 500). $BaSO_4$ was used as a reflectance standard. Morphology of the samples was characterized by field emission scanning electron microscopy (SEM) (JSM-6700F). The generation of $^{\bullet}OH$ radicals was investigated by the method of photoluminescence with terephthalic acid [17]. The $^{\bullet}OH$-trapping photoluminescence spectra were surveyed by an Edinburgh FL/FS900 spectrophotometer.

2.3. Photocatalytic activity measurements

Photocatalytic reactions were performed in a quartz tube with 4 cm inner diameter and 17.7 cm length. Three 4 W UV lamps with a wavelength centered at 254 nm (Philips, TUV4W/G4 T5) were used as illuminating source. One hundred milligrams of powdered photocatalyst was suspended in 150 mL of salicylic acid aqueous solution (2.5×10^{-4} mol/L) and Rhodamine B aqueous solution (1×10^{-5} mol/L). Vigorous stirring and oxygen bubbling (20 mL/min) were set up during this photocatalytic process. Before irradiation the suspension was stirred in the dark for 2 h to ensure the adsorption/desorption equilibrium. A 3 mL aliquot was taken at 15 min intervals during the experiment and centrifuged. The resulting clear liquor was analyzed on a Varian Cary-50 UV–vis-NIR spectrophotometer. The percentage of degradation was reported as C/C_0 where C was the absorption of salicylic acid and Rhodamine B at each irradiated time interval of the main peak of the absorption spectrum and C_0 was the absorption of the starting concentration when adsorption/desorption equilibrium was achieved.

2.4. Theoretical calculations

The structural optimizations for $PbMoO_4$ and $SrMoO_4$ were performed by using the projector-augmented wave (PAW) formalism of density functional theory (DFT), as implemented in the *Vienna ab initio* simulations package (VASP) [18,19], and the Perdew–Burke–Ernzerhof (PBE) type exchange correlation was adopted. In the calculations, the cell shape and the atomic positions were allowed to be relaxed at an energy cutoff of 500 eV and a $3 \times 3 \times 3$ Monkhorst-Pack k-point grid. To evaluate the atomic contribution to electronic structure, further calculations based on the linear combination of atomic orbital (LCAO) were carried out to obtain the information about the band structures and density of states (DOSs). In the calculations, Hay and Wadt's relativistic effective core potentials (RECPs) were used for Pb, Mo and Sr atoms [20,21], and a 8-411G(d) basis set was adopted for oxygen atoms [22]. To obtain the good prediction of band gap [23], Becke's three-parameter hybrid functional (B3LYP) was used in this stage. All the band–structure calculations were performed by using the CRYSTAL program in the structures optimized by PAW calculations [24]. Our previous investigations indicated that this two-step procedure could produce reasonable results [25].

3. Results and discussion

3.1. XRD analyses and Brunauer–Emmett–Teller (BET) surface areas

Fig. 2 shows the XRD patterns of $PbMoO_4$ prepared by the solvothermal process at various pH values and solid-state sintering. The pure-phase $PbMoO_4$ is a tetragonal structure, and the corresponding JCPDS number is 44-1486. The peaks at 17.8°, 27.5°, 29.5°, 37.8°, 40.8°, 43.5°, 44.9°, 47.4°, 51.2°, 55.6°, 56.8° match well with the (1 0 1), (1 1 2), (0 0 4), (1 1 4), (1 0 5), (1 2 3), (2 0 4), (2 2 0), (1 1 6), (3 1 2), (2 2 4) crystal planes of wulfenite $PbMoO_4$. The samples prepared by the solvothermal process at various pH values show different peak intensities. It may be due to the anisotropic growth of different crystal planes under different synthesis conditions. The X-ray diffraction pattern of $SrMoO_4$ prepared by the solvothermal process is shown in Fig. 3. All peaks are attributed to those of $SrMoO_4$ (JCPDS 85-0586). The average crystallite sizes of all samples are calculated by Scherrer equation as shown in Table 1. When pH <11, the prepared $PbMoO_4$ samples by solvothermal process show similar crystallite sizes with about 42–49 nm, while, when pH value increases to 11, the sample shows the largest crystallite size about 71.6 nm. Compared the crystallite sizes between sample $PbMoO_4$ (CS-9) and $SrMoO_4$ (CS-9), they exhibit similar crystallite sizes. BET surface areas as one of the important factors affecting photocatalytic activity are listed in Table 1.

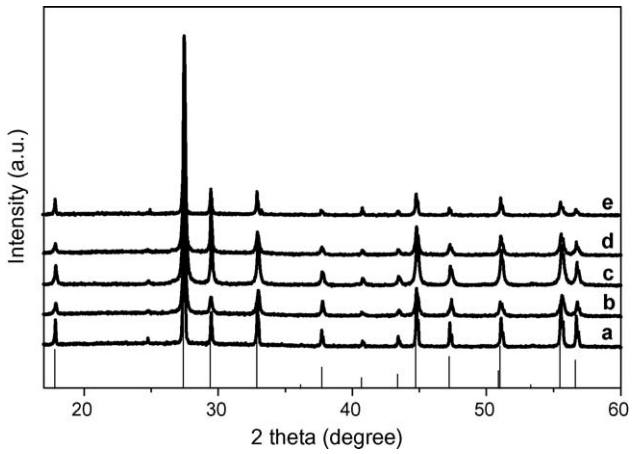

Fig. 2. X-ray diffraction patterns of $PbMoO_4$ samples: (a) $PbMoO_4$ (CS-5) (b) $PbMoO_4$ (CS-7) (c) $PbMoO_4$ (CS-9) (d) $PbMoO_4$ (CS-11) (e) $PbMoO_4$ (SS).

3.2. UV–vis diffuse reflectance spectra

Fig. 4 shows the diffuse reflection spectra of $PbMoO_4$ samples. The wavelength at the absorption edge, λ, is determined as the intercept on the wavelength axis for a tangent line drawn on absorption spectra. The absorption for all these samples locates at ca. 378 nm, corresponding to band gap energy of about 3.3 eV. The absorption edge of the samples prepared by the solvothermal process blue-shift compared to that of the sample prepared by the solid-state sintering. It can be observed that sample $PbMoO_4$ (CS-5) exhibits a little absorption at the visible region in agreement with the brown color of the sample. Compared the diffuse reflection spectrum of sample $PbMoO_4$ (CS-9) with that of sample $SrMoO_4$ (CS-9) as shown in Fig. 5, it can be observed that $SrMoO_4$ (CS-9) displays a shorter absorption edge of 281 nm corresponding to a band gap of 4.4 eV.

3.3. SEM images

Typical SEM micrographs of $PbMoO_4$ and $SrMoO_4$ samples are shown in Fig. 6. It can be observed that the particles agglomerate when pH is 5 (Fig. 6a). With the pH value increasing to 7 and 9, the morphologies keep unchanged (Fig. 6b and c). When the pH value increases to 11, the regular 18-facet polyhedron can be clearly observed (Fig. 6d), which are very similar to the results obtained in the study of $PbWO_4$ [26]. The surface of the crystals is very smooth. It is thought that in very strong basic precursor solution, a number of OH^- ions selectively adsorbed on different crystallographic planes. The activities of the planes with sufficient OH^- ions were reduced, and growth rates in some certain directions were confined. These led to the anisotropic growth process [27] and a number of 18-facet polyhedron particles formed. While the sample prepared by the solid-state sintering exhibits a coarse particle agglomerates of irregular morphology with a wide size distribution (Fig. 6f). The prepared $SrMoO_4$ sample shows the similar morphology to sample $PbMoO_4$ (CS-5) but a higher dispersion (Fig. 6e).

Table 1
Crystallite sizes and BET surface areas of $PbMoO_4$ and $SrMoO_4$ samples.

Sample	Crystallite size (nm)	BET (m^2/g)
$PbMoO_4$ (CS-5)	46.2	5.5
$PbMoO_4$ (CS-7)	48.5	12.0
$PbMoO_4$ (CS-9)	42.4	12.4
$PbMoO_4$ (CS-11)	71.6	0.6
$PbMoO_4$ (SS)	56.6	0.2
$SrMoO_4$ (CS-9)	42.8	10.5

3.4. Photocatalytic activity

The photocatalytic activities of the samples were evaluated by the degradation of salicylic acid. Fig. 7 displays the concentration changes of salicylic acid at 297 nm as a function of irradiation time during the degradation process. Compared the photocatalytic activity between $SrMoO_4$ sample and $PbMoO_4$ sample, it can be observed that $SrMoO_4$ sample exhibits a negligible photocatalytic activity. For $PbMoO_4$ samples prepared by solvothermal process with the increase of pH value the activity increases. The highest photocatalytic activity is obtained by sample $PbMoO_4$ (CS-11) (Fig. 7f). The salicylic acid can be decomposed totally within 150 min. While the conversion mediated by the samples prepared at pH 5, pH 7 and pH 9 is about 40% (Fig. 7b), 80% (Fig. 7d) and 90% (Fig. 7e) respectively. The sample prepared by solid-state sintering displays a conversion of 40% (Fig. 7c) and its photocatalytic activity is far lower than that of the samples prepared by the solvothermal process except sample $PbMoO_4$ (CS-5). In order to quantitatively understand the reaction kinetics of the salicylic acid degradation in

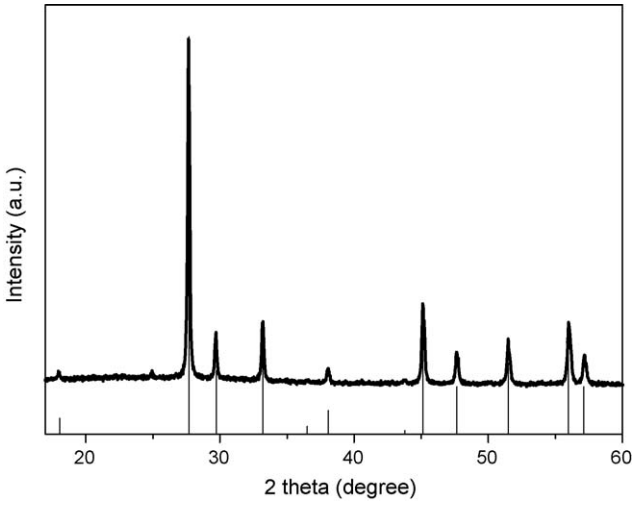

Fig. 3. X-ray diffraction pattern of $SrMoO_4$ sample prepared by solvothermal process at pH 9.

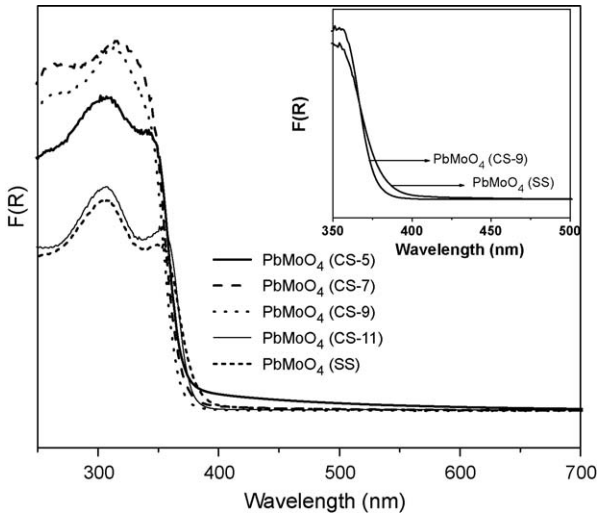

Fig. 4. Diffuse reflectance absorption spectra of $PbMoO_4$ samples.

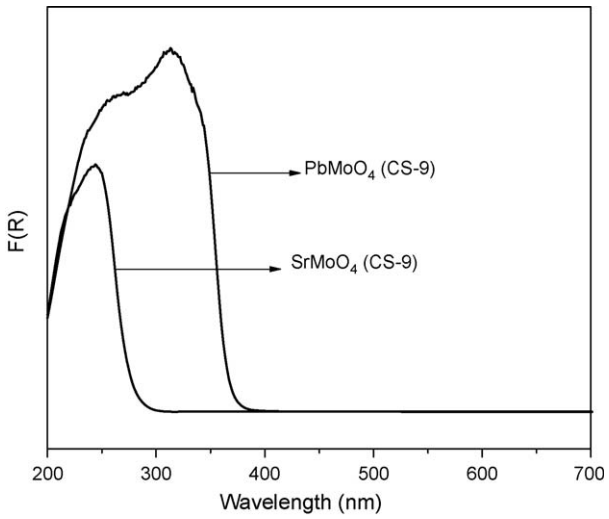

Fig. 5. Diffuse reflectance absorption spectra of $SrMoO_4$ (CS-9) and $PbMoO_4$ (CS-9).

our experiments, we applied the pseudo-first order model as expressed by Eq. (1), which is generally used for photocatalytic degradation process if the initial concentration of pollutant is low [28]:

$$\ln(C_0/C) = kt \quad (1)$$

where C_0 and C are the concentrations of the pollutants in solution at time 0 and t, respectively, and k is the pseudo-first order rate constant. Fig. 8 is the photocatalytic reaction kinetics of salicylic acid degradation in solution based on the data plotted in Fig. 7. The rate constants obtained from the regression lines in Fig. 8 are included in Table 2. As can be observed, a fairly good correlation to the pseudo-first order reaction kinetics ($R > 0.98$) was found. The salicylic acid removal rate over $PbMoO_4$ (CS-11) (Fig. 7a) is about 4 times as high as that over $PbMoO_4$ (SS) (Fig. 8e). $SrMoO_4$ (CS-9) is nearly inactive and it does not follow the pseudo-first order model.

To investigate the photoactivity of $PbMoO_4$ and $SrMoO_4$ toward other organic compounds, Rhodamine B was employed. As shown in Fig. 9, Rhodamine B can be degraded almost completely after 40 min irradiation with UV light by sample $PbMoO_4$ (CS-9), while sample $SrMoO_4$ (CS-9) shows a much lower photocatalytic activity. The photocatalytic activities in gas phase of these two samples are also examined. It is found that sample $PbMoO_4$ (CS-9) also shows a higher photocatalytic activity for the decomposition of benzene than $SrMoO_4$ (CS-9). These two photocatalytic reactions further confirm the effectiveness of the solvothermally prepared $PbMoO_4$ sample compared to $SrMoO_4$.

The stability of a photocatalyst is very important for its application. Herein, the stability of $PbMoO_4$ was investigated via the decomposition of salicylic acid. The lifetime for $PbMoO_4$ is shown in Fig. 10. The results reveal that the sample does not exhibit obvious loss of activity.

The leaching of Pb ions from $PbMoO_4$ catalyst during the photocatalytic reaction is also examined by inductively coupled plasma (ICP) method. The concentration of Pb ions is 0.14 mg/L after 4 h irradiation under UV light. It satisfies the wastewater discharge standard. Therefore it is thought that the effect of little dissolution of Pb ions on the application of $PbMoO_4$ catalyst in the water purification can be negligible.

Table 2
The pseudo-first order rate constants of salicylic acid photodecomposition over $PbMoO_4$ catalysts.

Sample	k (min^{-1})	R
$PbMoO_4$ (CS-5)	0.0024	0.9931
$PbMoO_4$ (CS-7)	0.0058	0.9963
$PbMoO_4$ (CS-9)	0.0076	0.9961
$PbMoO_4$ (CS-11)	0.0105	0.9863
$PbMoO_4$ (SS)	0.0024	0.9889

3.5. •OH-trapping photoluminescence spectra

In the photocatalytic process, the photo-generated holes can react with adsorbed water to form •OH radicals which are the major active oxidation species in the decomposition of organic pollutes. Terephthalic acid was used to readily react with •OH to form highly fluorescent products, 2-hydroxyterephthalic acid which can be detected by fluorescence spectrum (excitation wavelength: 312 nm, fluorescence peak: 426 nm) [17]. From the fluorescence intensity, the amount of •OH radical could be estimated. Fig. 11 shows the •OH-trapping photoluminescence spectra of sample $PbMoO_4$ (CS-9) in a terephthalic acid solution at room temperature under UV-light irradiation. This implies that fluorescent products formed during the photocatalytic process which is due to the specific reaction between •OH and terephthalic acid. The fluorescence intensity at 426 nm increases when UV light is irradiated continuously. The stronger fluorescence intensity means the more •OH is produced. As the relation between fluorescence intensity and irradiation time is linear, the formed •OH is proportional to irradiation time (inset in Fig. 11). The generated rate of •OH can be calculated by the slope of straight lines in the inset of Fig. 11. It exhibits that the linear slope of the change in fluorescence intensity for sample $PbMoO_4$ (CS-9) are steeper than that for sample $SrMoO_4$ (CS-9) suggesting that the greater formation rate of •OH radical was produced over sample $PbMoO_4$ (CS-9). The greater the formation rate of •OH radicals is the higher separation efficiency of electron–hole pairs is achieved. Therefore the higher photocatalytic activity can be observed on sample $PbMoO_4$ (CS-9).

3.6. Electronic structure calculations

The bulk structures of $PbMoO_4$ and $SrMoO_4$ have been reported as scheelite-type structure with space group $I4_1/a$, and are characterized by two lattice parameters a and c. In this structure, the Mo atom is four-fold coordinated with surrounding oxygen atoms and the MoO_4 tetrahedral units are observed. For $PbMoO_4$, the optimized cell parameters are $a = 5.511$ Å and $c = 12.346$ Å, which are in agreement with the experimental values of $a = 5.431$ Å and $c = 12.107$ Å [29]. The predicted Mo–O bond lengths in MoO_4 tetrahedral are 1.800 Å and the nearest Pb–O distance is about 2.655 Å. When Pb atoms are replaced by Sr atoms, the cell volume of $SrMoO_4$ is slightly changed. The calculated lattice parameters of $SrMoO_4$ are 5.486 and 12.235 Å for a and c, respectively. These values are also consistent with the experimental values of 5.394 and 12.02 Å [30]. It is noted that the replacement of Pb^{2+} ion by Sr^{2+} has negligible influence on the structure of MoO_4 tetrahedral, and nearly identical Mo–O bond length (1.798 Å) is obtained in $SrMoO_4$. Moreover, the length of the shortest Sr–O bond (2.617 Å) is also similar to the value of Pb–O bond.

The B3LYP hybrid DFT method was carried out to determine the electronic structures of $PbMoO_4$ and $SrMoO_4$, and their band structures are displayed in Fig. 12. Although the structures of two compounds are very similar, some obvious differences are observed by examining their band structures. For $PbMoO_4$, an indirect transition from the valence band at the point near M to the conduction band at X as the minimum band gap with a value of 4.00 eV is predicted, while a larger direct band gap (5.29 eV) is found at Γ point for $SrMoO_4$. Another difference is that, $PbMoO_4$

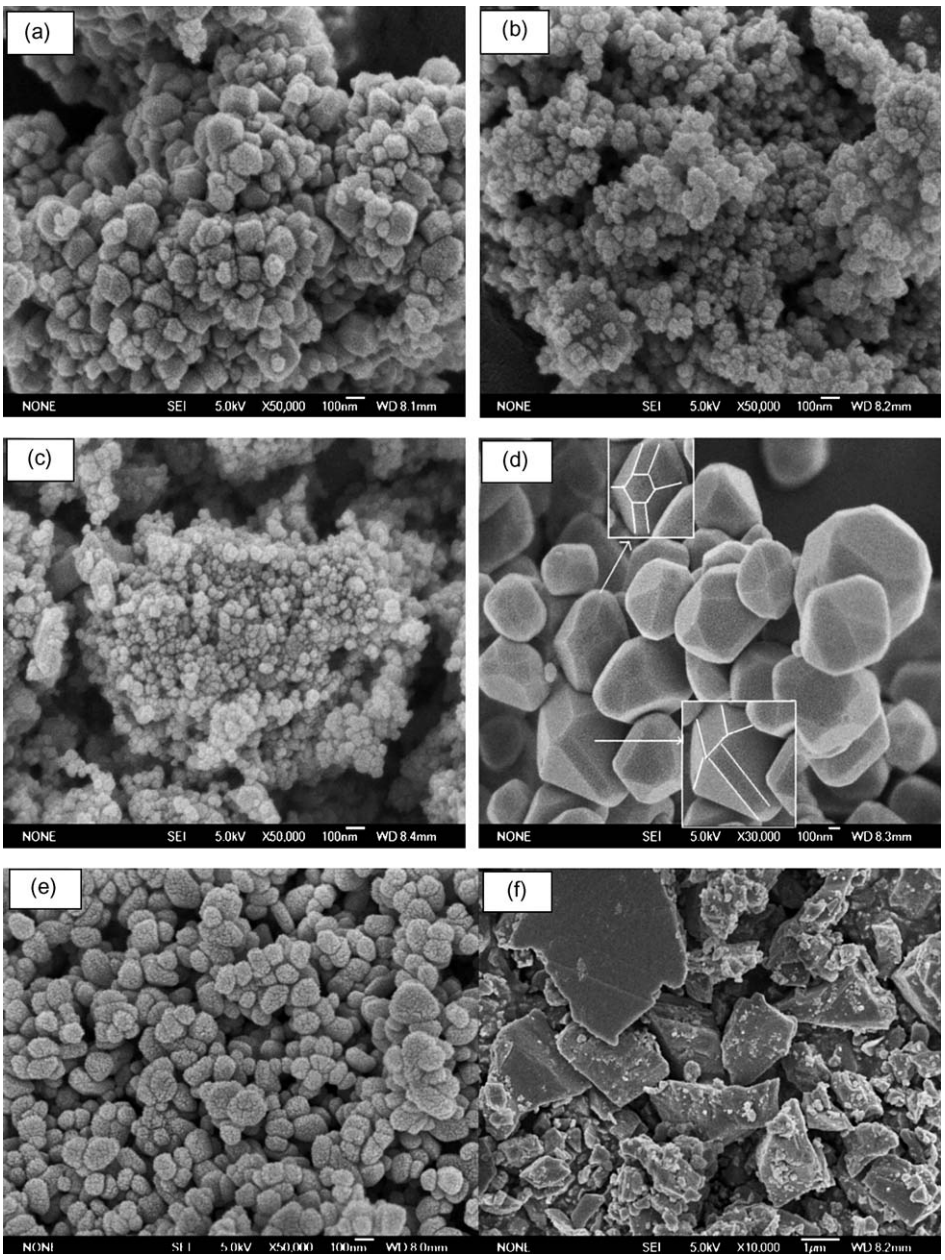

Fig. 6. SEM images of $PbMoO_4$ and $SrMoO_4$ samples prepared by the solvothermal process and the solid-state process: (a) $PbMoO_4$ (CS-5) (b) $PbMoO_4$ (CS-7) (c) $PbMoO_4$ (CS-9) (d) $PbMoO_4$ (CS-11) (e) $SrMoO_4$ (CS-9) (f) $PbMoO_4$ (SS).

shows larger dispersions of both the valence and conduction bands with respect to the case of $SrMoO_4$. This means that the electrons or holes in $PbMoO_4$ are more delocalized than in $SrMoO_4$. In other word, the generated holes and electrons on $PbMoO_4$ exhibit a larger mobility leading to a slow recombination. Therefore for $PbMoO_4$ more photo-generated holes can react with absorbed water to form larger amount of $^{\bullet}OH$ radical in the photocatalytic process. It is consistent with the result of $^{\bullet}OH$-trapping photoluminescence spectra.

In order to explain the differences between two band structures, the atomic DOSs of $PbMoO_4$ and $SrMoO_4$ are also calculated and the results are presented in Fig. 13. Because of the obvious dispersions of the energy bands, the widths of valence and conduction band of $PbMoO_4$ are larger than those of $SrMoO_4$. As shown in Fig. 13, the conduction bands of two compounds are dominated by Mo 4d states and some contributions of Pb(Sr) and O atoms are also observed. However, it is worthwhile to note that the components of the top of valence band are different. For $SrMoO_4$, like many metal oxides, the top of the valence band is mainly derived from O 2p states. On the other hand, the top of the valence band of $PbMoO_4$ consists of not only O 2p but also Pb 6s states, indicating the obvious covalent interactions between Pb and O atoms. This is agreement with the report about $PbMoO_4$ by Kudo and co-workers [9].

Fig. 14 presents the contour plots of the difference charge density maps for two compounds, which are defined as the difference between the total electron density and linear superposition of radially symmetric atomic charge densities. Here, we only focus the charge distributions around Pb (or Sr) atom and the plane displayed in Fig. 14 contains two Pb–O (or Sr–O) bonds. For $PbMoO_4$, the charge densities around Pb atom do not maintain spherical shape, and one therefore expects a considerable degree of

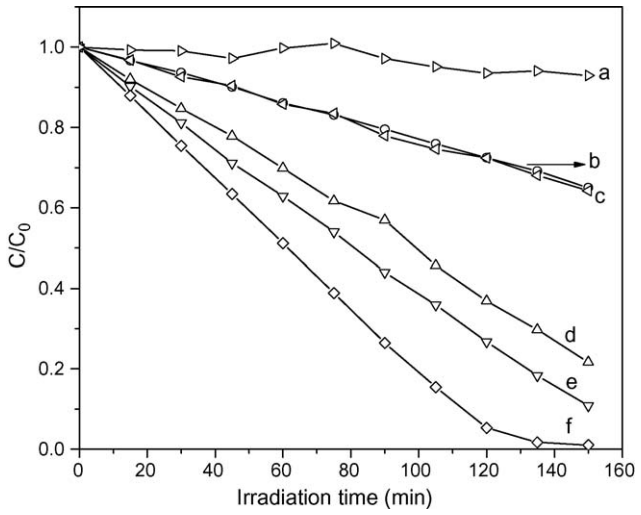

Fig. 7. Concentration changes of salicylic acid (2.5×10^{-4} M) at 297 nm as a function of irradiation time during the degradation process ($\lambda = 254$ nm): (a) $SrMoO_4$ (CS-9) (b) $PbMoO_4$ (CS-5) (c) $PbMoO_4$ (SS) (d) $PbMoO_4$ (CS-7) (e) $PbMoO_4$ (CS-9) (f) $PbMoO_4$ (CS-11).

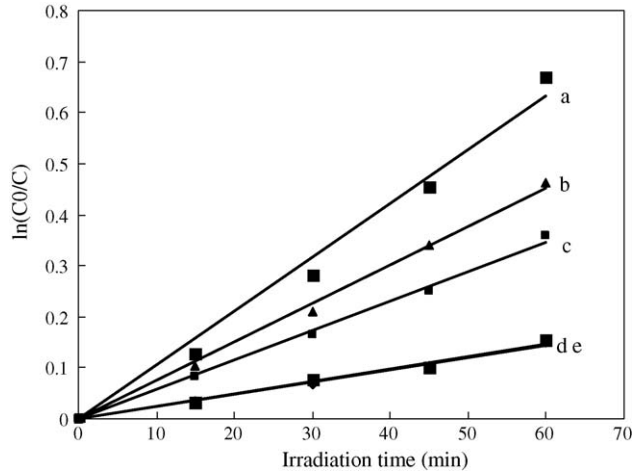

Fig. 8. Kinetics of salicylic acid removal in solutions: (a) $PbMoO_4$ (CS-11) (b) $PbMoO_4$ (CS-9) (c) $PbMoO_4$ (CS-7) (d) $PbMoO_4$ (CS-5) (e) $PbMoO_4$ (SS).

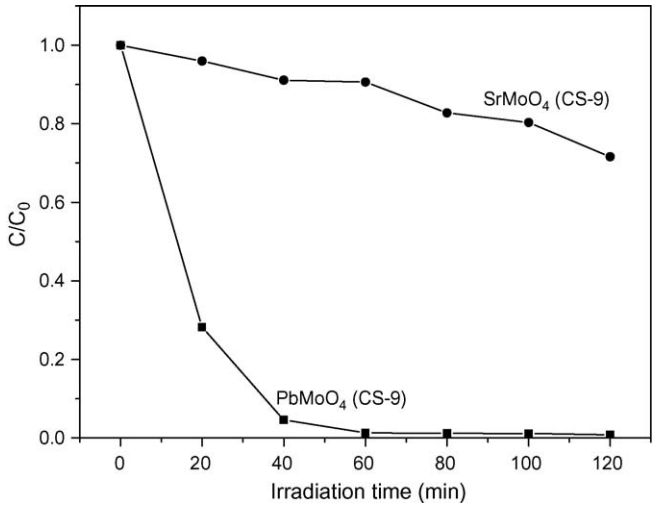

Fig. 9. Concentration changes of Rhodamine B at 554 nm as a function of irradiation time in the presence of sample $PbMoO_4$ (CS-9) and $SrMoO_4$ (CS-9).

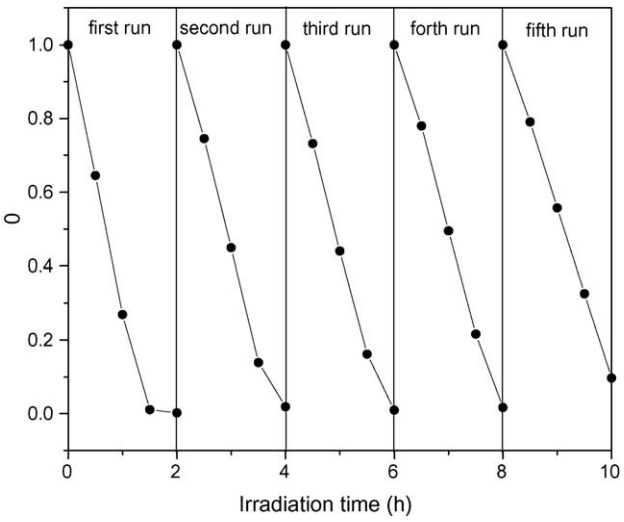

Fig. 10. The lifetime for photodegradation of salicylic acid on $PbMoO_4$ (CS-11) sample.

covalent character between Pb and O atoms. However, the charge densities tend to exhibit spherical distribution around Sr atom for $SrMoO_4$. The atomic-like charge densities surrounding Sr atom imply that the ionic bonding becomes the predominant character of the Sr–O bonds.

According to the above discussions, it is clear that larger dispersion of energy band observed for $PbMoO_4$ is related to the covalent interactions between Pb and O atoms. In addition, the obvious hybridization of Pb 2s and O 2p states will introduce some "split-off" states [2] appeared in the band gap, and consequently, a narrow band gap is expected for $PbMoO_4$ compared to $SrMoO_4$. This agrees well with the result of DRS as shown in Fig. 4. Actually, a narrower band gap has also been observed for other compounds with similar electronic structure, such as $Sn_2Ta_2O_7$ [31], $PbWO_4$ [2] and so forth.

3.7. Discussion

$SrMoO_4$ and $PbMoO_4$ have the similar crystal structure. In their structure, the Mo atom is four-fold coordinated with surrounding oxygen atoms and the MoO_4 tetrahedral units are observed. In the

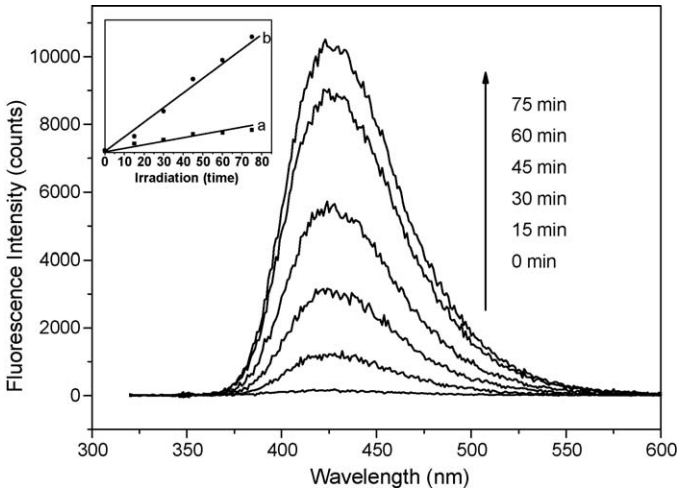

Fig. 11. •OH-trapping photoluminescence spectra of $PbMoO_4$ (CS-9) in a solution of terephthalic acid at room temperature (excitation at 312 nm, emission at 426 nm). Inset: Plot of the induced fluorescence intensity at 426 nm against irradiation time: (a) $SrMoO_4$ (CS-9) (b) $PbMoO_4$ (CS-9).

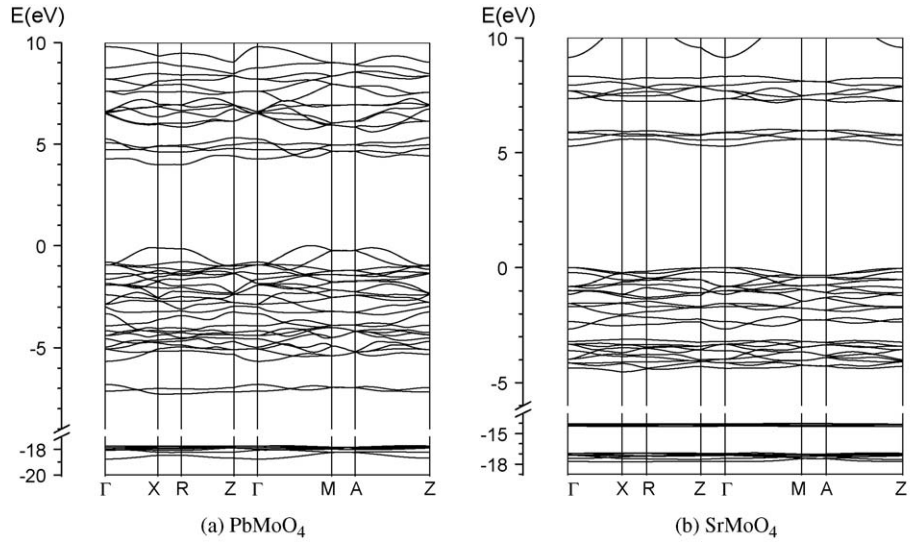

Fig. 12. Band structures of $PbMoO_4$ and $SrMoO_4$ calculated by the B3LYP hybrid DFT method. The valence-band maximum is taken as the energy zero.

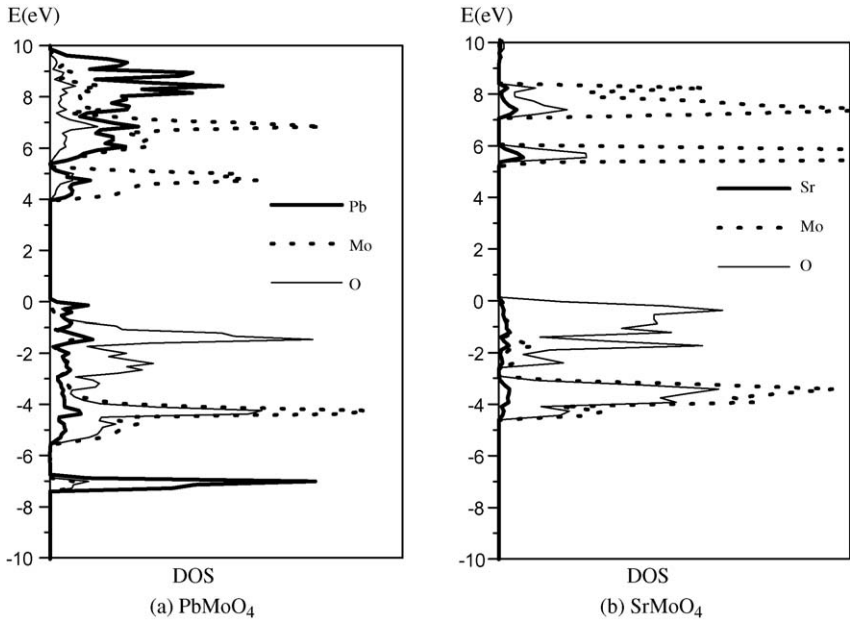

Fig. 13. Atomic partial DOSs of $PbMoO_4$ and $SrMoO_4$. The valence-band maximum is taken as the energy zero.

decomposition of salicylic acid, Rhodamine B and benzene experiment $PbMoO_4$ exhibits a high photocatalytic activity, while $SrMoO_4$ displays a negligible photocatalytic activity. It can be deduced that the photocatalytic activity is not induced by MoO_4 tetrahedron. As known geometric structure of the photocatalyst also greatly influences the photocatalytic activity. Using the crystallographic data regarding the atom positions, we have calculated the center of gravity of oxygen ions surrounding a Mo^{6+} ion and Pb^{2+} or Sr^{2+} for $PbMoO_4$ and $SrMoO_4$. The calculations show that $PbMoO_4$ and $SrMoO_4$ are constituted by MoO_4 tetrahedron and PbO_8 or SrO_8 dodecahedron both of which do not deviate from the position of Mo^{6+} ion and Pb^{2+} or Sr^{2+} ions. Therefore the difference of photocatalytic activity between $PbMoO_4$ and $SrMoO_4$ is not induced by the crystal structure and geometric structure. BET surface area is another important factor in photocatalysis. $SrMoO_4$ (CS-9) and $PbMoO_4$ (CS-9) prepared under the same synthesis condition exhibit the similar BET surface areas as shown in Table 1. Therefore the effect of surface areas on the photocatalytic activity is also excluded. Via DFT calculations, it is found that the electronic structures between $PbMoO_4$ and $SrMoO_4$ exhibit obvious differences. $PbMoO_4$ shows larger dispersions of both the valence and conduction bands with respect to the case of $SrMoO_4$ due to Pb^{2+} with $d^{10}s^2$ configuration which is similar to the reported splitting water material $PbWO_4$ [2]. The larger dispersions in the conduction band and valence band are good for the mobility of photogenerated carriers and lead to a higher separation efficiency of electron–hole pairs as confirmed by the result of $^{\bullet}OH$-trapping photoluminescence spectra. Therefore $PbMoO_4$ shows far higher photocatalytic activity than that of $SrMoO_4$. For the samples prepared by the solvothermal process, the highest photocatalytic activity was obtained by sample $PbMoO_4$ (CS-11) though its BET surface area is lowest among these $PbMoO_4$ samples. From the result of SEM, it can be found that the surface of the particles of $PbMoO_4$ (CS-11) is very smooth and the particles are very perfect. It

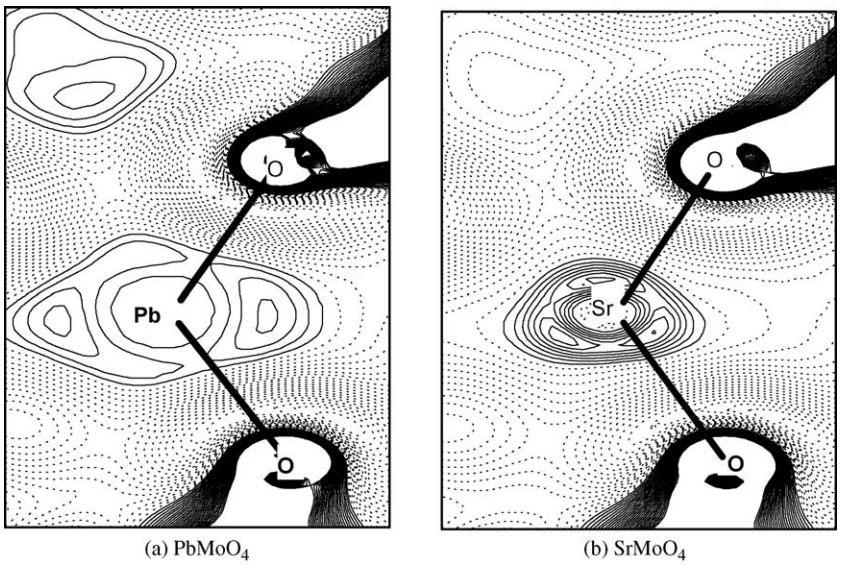

Fig. 14. Different charge density maps for $PbMoO_4$ and $SrMoO_4$. The plane shown in figure contains two Pb(Sr)–O bonds, and the solid and dotted lines indicate the increasing and decreasing of the charge densities, respectively.

is thought that its crystal (bulk) defect is lower than that of other samples prepared at different pH values (5, 7, 9). Less crystal defects can diminish the recombination of photo-generated carriers. In addition, surface states would exist on the rough surface. The surface states trap a part of photo-generated electrons and holes, and decrease their reduction and oxidation potentials, and further work as recombination centers [31]. Therefore sample $PbMoO_4$ (CS-11) shows a higher photocatalytic activity than other samples. Common problems in the solid-state process include the uncontrollably large grain growth, localized segregation of the particles, and possible loss of stoichiometry due to volatilization of the constituent components at high temperatures, all of which result in a decrease in the photocatalytic activity compared to the soft chemical process. Therefore $PbMoO_4$ (SS) exhibits a lower photocatalytic activity. While sample $PbMoO_4$ (CS-5) shows the similar photocatalytic activity to the sample prepared by the solid-state sintering. As mentioned above sample $PbMoO_4$ (CS-5) exhibits a brown color and a little absorption at visible range. It was thought that in the acidic situation, ethylene glycol may be oxidized to carbon or carbonaceous residues and then covers around the catalyst. A part of light is blocked off and cannot excite the catalyst. The few photo-generated carriers and its lower BET surface area lead to the lower photocatalytic activity. The sample after the photocatalytic examination is characterized by XRD. It can be observed that the crystal structure of the sample remains unchanged after the photocatalytic examination proving that the photocatalytic activity is really induced by the photocatalytic reaction rather than the reaction between catalyst and salicylic acid as shown in Fig. 15.

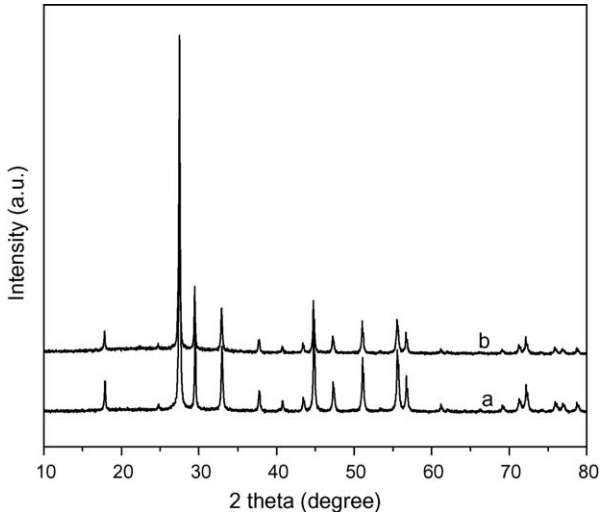

Fig. 15. X-ray diffraction patterns of sample $PbMoO_4$ (CS-7): (a) before activity (b) after activity.

4. Conclusions

$PbMoO_4$ and $SrMoO_4$ particles are successfully synthesized by a simple solvothermal process. The results of UV–vis DRS show all $PbMoO_4$ samples exhibit a band gap of about 3.3 eV, while $SrMoO_4$ shows a larger band gap of about 4.4 eV. Photocatalytic evaluation via the decomposition of salicylic acid under the irradiation of UV light reveals that $PbMoO_4$ samples obtained under different conditions exhibit different photocatalytic performances and the highest photocatalytic activity is obtained by the sample prepared at pH 11. All $PbMoO_4$ samples prepared by the solvothermal process show higher photocatalytic activities than the sample prepared by the solid-state sintering except the sample prepared at pH 5 and their rate constants are larger than that of the solid-state reaction synthesized $PbMoO_4$ via the use of pseudo-first order model. Compared to $SrMoO_4$ with the same crystal structure to $PbMoO_4$, $PbMoO_4$ displays a far higher photocatalytic activity for the decomposition of salicylic acid, Rhodamine B and benzene under UV light irradiation. By DFT calculations, it is found that the electronic structures between $PbMoO_4$ and $SrMoO_4$ are very different. The valence and conduction bands of $PbMoO_4$ exhibit larger dispersions due to the existence of Pb^{2+} than that of $SrMoO_4$. The larger band dispersions are in favor of the separation of the photo-generated holes and electrons leading to more active radicals $^{\bullet}OH$ which is confirmed by the $^{\bullet}OH$-trapping photoluminescence spectra. Therefore, $PbMoO_4$ shows a higher photocatalytic activity than $SrMoO_4$.

Acknowledgements

The work was supported by National Natural Science Foundation of China (20777011, 20773024 and 20537010), National Key

Basic Research Program of China (973 Program: 2007CB613306 and 2008CB617507), Specialized Research Fund for the Doctoral Program of Higher Education of China (20060386001) and Program for Changjiang Scholars and Innovative Research Team in University (PCSIRT0818).

References

[1] K.L. Zhang, C.M. Liu, F.Q. Huang, C. Zheng, W.D. Wang, Appl. Catal. B: Environ. 68 (2006) 125–129.
[2] H. Kadowaki, N. Saito, H. Nishiyama, H. Kobayashi, Y. Shimodaira, Y. Inoue, J. Phys. Chem. C 111 (2007) 439.
[3] M. Ishii, M. Kobayashi, Prog. Cryst. Growth Charact. 23 (1991) 245.
[4] N. Faure, C. Borel, M. Couchaud, G. Basset, R. Templier, C. Wyon, Appl. Catal. B: Environ. 63 (1996) 593.
[5] G. Angloher, C. Bucci, C. Cozzini, F. Feilitzsch, T. Frank, D. Hauff, S. Henry, Th. Jagemann, J. Jochum, H. Kraus, B. Majorovits, J. Ninkovie, F. Petricca, et al. Nucl. Instrum. Methods Phys. Res. A 520 (2004) 108.
[6] E.F. Paski, M.W. Blades, Anal. Chem. 60 (1988) 1224.
[7] E.R.S. Daniel, X.H. Kumar, C.Y. Ma, J. Tu, Solid State Chem. 181 (2008) 355–364.
[8] A. Kudo, M. Steinberg, A.J. Bard, A. Campion, M.A. Fox, T.E. Mallouk, S.E. Webber, J.M. White, Catal. Lett. 5 (1990) 61.
[9] Y. Shimodaira, H. Kato, H. Kobayashi, A. Kudo, Bull. Chem. Soc. Jpn. 80 (2007) 885.
[10] S. Sabharwal, C. Sangeeta, D.G. Desai, Cryst. Growth Des. 6 (2006) 59.
[11] H.C. Zeng, J. Cryst. Growth 171 (1997) 136.
[12] G.H. Jia, C.Y. Tu, Z.Y. You, J.F. Li, Z.J. Zhu, Y. Wang, B.C. Wu, J. Cryst. Growth 273 (2004) 220.
[13] Y. Cheng, Y.S. Wang, D. Chen, F. Bao, J. Phys. Chem. B 109 (2005) 794.
[14] J.C. Sczancoski, L.S. Cavalcante, M.R. Joya, J.A. Varela, P.S. Pizani, E. Longo, Chem. Eng. J. 140 (2008) 632–637.
[15] J.H. Bi, L. Wu, J. Li, Z.H. Li, X.X. Wang, X.Z. Fu, Acta Mater. 55 (2007) 4699.
[16] B. Muktha, T.N. Giridhar Madras, Guru Row, J. Photochem. Photobiol. A 187 (2007) 177–185.
[17] Q. Xiao, Z.C. Si, J. Zhang, C. Xiao, X.K. Tan, J. Hazard. Mater. 150 (2008) 62–67.
[18] G. Kresse, J. Furthmuller, Phys. Rev. B 54 (1996) 11169.
[19] G. Kresse, J. Furthmuller, Comput. Mater. Sci 6 (1996) 15.
[20] S. Piskunov, E. Heifets, R.I. Eglitis, G. Borstel, Comput. Mater. Sci. 29 (2004) 165.
[21] F. Corà, A. Patel, N.M. Harrison, C. Roetti, C.R.A. Catlow, J. Mater. Chem. 7 (1997) 959.
[22] F. Corà, Mol. Phys. 103 (2005) 2483.
[23] J. Muscat, A. Wander, N.M. Harrison, Chem. Phys. Lett. 342 (2001) 397.
[24] V.R. Saunders, R. Dovesi, C. Roetti, M. Causa, N.M. Harrison, R. Orlando, C.M. Zicovich-Wilson, CRYSTAL98 User Manual, University of Torino, Torino, 1998.
[25] W. Ling, Y.F. Zhang, Y. Li, K.N. Ding, J.Q. Li, Y.J. Xu, J. Chem. Phys. 124 (2006) 054704.
[26] J. Geng, J.J. Zhu, H.Y. Chen, Cryst. Growth Des. 6 (2006) 321–326.
[27] T. Thongtem, A. Phuruangrat, S. Thongtem, Curr. Appl. Phys. 8 (2008) 189–197.
[28] J.M. Herrmann, H. Ahiri, Y. Ait-Ichou, G. Lassaletta, A.R. Gonzalez-Elipe, A. Fernandez, Appl. Catal. B: Environ. 13 (1997) 219.
[29] J. Leciejewicz, Zeitschrift fuer Kristallographie 121 (1965) 158–164.
[30] E. Guermen, E. Daniels, J.S. King, J. Chem. Phys. 55 (1971) 1093–1097.
[31] Y. Hosogi, Y. Shimodaira, H. Kato, H. Kobayashi, A. Kudo, Chem. Mater. 20 (2008) 1299–1307.